NANO LETTERS

pubs.acs.org/NanoLett Letter

Photon Upconversion in a Vapor Deposited 2D Inorganic–Organic Semiconductor Heterostructure

Reynolds Dziobek-Garrett,[‖] Christian J. Imperiale,[‖] Mark W.B. Wilson,* and Thomas J. Kempa*

Cite This: *Nano Lett.* 2023, 23, 4837–4843 Read Online

ACCESS | Metrics & More | Article Recommendations | Supporting Information

ABSTRACT: Energy transfer processes may be engineered in van der Waals heterostructures by taking advantage of the atomically abrupt, Å-scale, and topologically tailorable interfaces within them. Here, we prepare heterostructures comprised of 2D WSe_2 monolayers interfaced with dibenzotetraphenylperiflanthene (DBP)-doped rubrene, an organic semiconductor capable of triplet fusion. We fabricate these heterostructures entirely through vapor deposition methods. Time-resolved and steady-state photoluminescence measurements reveal rapid subnanosecond quenching of WSe_2 emission by rubrene and fluorescence from guest DBP molecules at 612 nm (λ_{exc} = 730 nm), thus providing clear evidence of photon upconversion. The dependence of the upconversion emission on excitation intensity is consistent with a triplet fusion mechanism, and maximum efficiency (linear regime) of this process occurs at threshold intensities as low as 110 mW/cm^2, which is comparable to the integrated solar irradiance. This study highlights the potential for advanced optoelectronic applications employing vdWHs which leverage strongly bound excitons in monolayer TMDs and organic semiconductors.

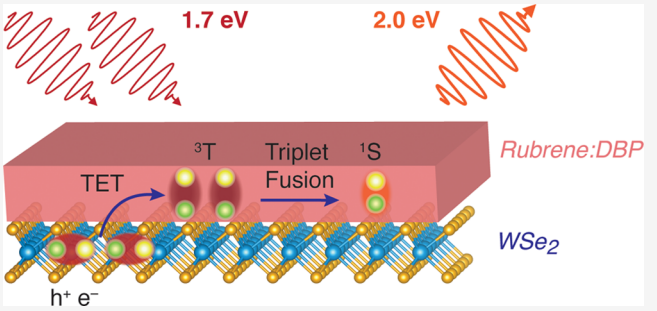

KEYWORDS: *upconversion, van der Waals heterostructure, 2D material, time-resolved photoluminescence, exciton,, triplet fusion*

Van der Waals heterostructures (vdWHs) comprised of stacked 2D crystal monolayers can be used to elicit emergent electronic and photonic phenomena.[1−4] For example, excitons in a 2D semiconductor can be significantly perturbed through altered band alignments and Moiré effects induced by an adjacent 2D crystal layer interacting only across the van der Waals gap.[5−9] Moreover, energy transfer processes may be engineered via vdWHs by taking advantage of the atomically abrupt, Å-scale, and topologically tailorable interfaces within them.[10] However, interfaces formed solely between 2D atomic crystals are not a panacea for creating and controlling unique correlated systems. Alternatively, molecular assemblies and lattices provide compelling advantages, because they are eminently modifiable through chemical synthesis and derivatization.[11−13] Mixed-dimensional heterostructures combine the mechanical flexibility of 2D atomic crystals with the structural and electronic tunability of molecular materials to enable advanced excitonic devices.[14−16] Initial studies of 2D-organic heterostructures have demonstrated their promise in photovoltaics,[17,18] photodetectors,[19−21] and spin-selective charge transport.[22]

Exploiting solid-state triplet fusion upconversion (TUC) within hybrid TMD/organic semiconductor architectures has recently generated considerable interest among the optoelectronics community.[23] During TUC, pairs of low-energy photons are converted into high-energy photons via an incoherent process mediated by the triplet (spin 1) excited states of organic semiconductors.[24,25] Since direct photoexcitation of these triplet states is spin-forbidden, TUC architectures employ triplet sensitizers that strongly absorb light and transfer photoexcitations to the molecular triplet acceptor states.[24] Once two diffusing triplets encounter each other, their energy may be combined in an overall spin-conservative process called triplet fusion (or triplet−triplet annihilation).[26] This process can yield a higher-energy singlet on one molecular chromophore that emits the final short-wavelength photon, thus manifesting the TUC process. Notably, the long excited-state lifetimes of molecular triplet excitons[27−31] facilitate effective (bimolecular) upconversion at modest light intensities.[24,28,32−37] In addition, the extended diffusion lengths of triplet excitons within organic films[27−30] permit the design of solid-state devices at feasible scales.[32,33] There is significant demand for practically deployable solid-state TUC architectures to serve as inverse scintillators that sensitize photovoltaic devices or focal-plane arrays to sub-bandgap light, and a variety of strategies are being ex-

Received: January 31, 2023
Revised: May 10, 2023
Published: May 16, 2023

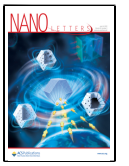

https://doi.org/10.1021/acs.nanolett.3c00380
Nano Lett. 2023, 23, 4837−4843

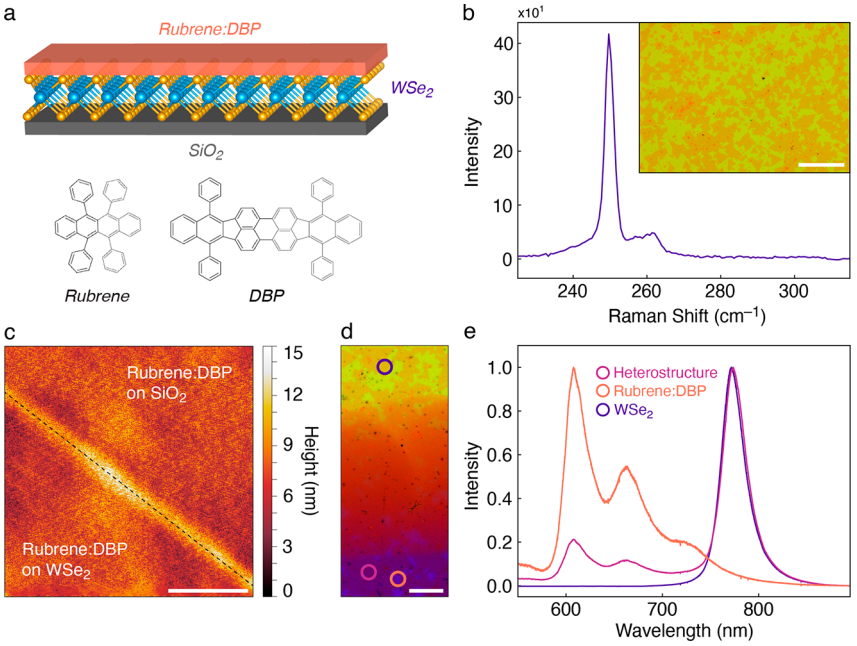

Figure 1. (a) Schematic (not to scale) of the monolayer 2D WSe_2 | rubrene heterostructure and chemical structures of rubrene and dibenzotetraphenylperiflanthene (DBP). (b) Raman spectrum of as-grown WSe_2. Inset: optical microscopy image of WSe_2 crystals grown atop a 200 nm SiO_2 on Si substrate; scalebar: 200 μm. (c) AFM map of a region of the sample showing uniform coverage of a 2D WSe_2 crystal and the adjacent bare SiO_2 substrate by rubrene; scalebar: 500 nm. (d) Optical microscope image (true-color) of the edge of the heterostructure. The dark purple region corresponds to the heterostructure (2D WSe_2 crystals covered by 60 nm rubrene:DBP), the red/orange region corresponds to the edge of the heterostructure which has a graded thickness of rubrene due to shadowing from the evaporation mask, and the uppermost region corresponds to the bare substrate with 2D WSe_2 crystals. The colored circles indicate the points from which the PL spectra shown in 'e' were recorded; scalebar: 100 μm. (e) PL spectra collected from the regions highlighted in 'd' for an excitation wavelength of 514 nm. The selected regions reveal emission from 2D WSe_2 (blue), rubrene:DBP (orange), and the 2D WSe_2 | rubrene heterostructure (purple).

plored.[23,32−34,38,39] Here, large-area 2D TMDs offer compelling advantages as triplet sensitizers, as they combine strong monolayer optical absorption,[40] spin-mixed band-edge states that minimize energy loss during triplet sensitization,[41] and Angstrom-scale physical proximity to molecular layers enabling fast energy transfer.[42]

This study highlights the emergent behaviors that can be engineered by interfacing molecular materials with long-lived triplet excitons with 2D atomic crystals and suggests that related architectures may have a transformative impact in photovoltaics, photodetection, sensing, and optical information processing.

To identify emergent properties in a 2D WSe_2-organic heterostructure (Figure 1a), we began by growing large-area films of monolayer 2D WSe_2 crystals (Figure 1a) via chemical vapor deposition (CVD; for methods see Supporting Information). Bright field optical microscopy (OM) images of these CVD grown samples reveal a uniform coverage of the SiO_2/Si substrate with crystals having edge lengths up to 100 μm (Figures 1b and S1). Raman spectra (Figure 1b) show clear E′ and A_1′ resonances at 249 and 261 cm^{-1}, respectively, that are consistent with those reported for monolayer WSe_2 of high crystallinity.[43] The extent of monolayer growth over the substrate area is discussed in more detail later in this section.

To complete the fabrication of our heterostructure, we deposited 60 nm of rubrene:DBP (rubrene doped with 1% dibenzotetraphenylperiflanthene, DBP)[44] directly onto selected regions of the as-grown 2D WSe_2 monolayers through an evaporation mask (Figure 1a). AFM scans of the deposited rubrene:DBP layer (Figures 1c and S2) do not exhibit signatures of ordering on length scales greater than our AFM lateral resolution of 10 nm. The surface is smooth, with no crystal grains apparent through ordered height variations or terraces. This result is consistent with other reports of room-temperature high-vacuum rubrene deposition[38−40] but is contrary to observations of crystalline pentacene formation on the surface of CVD-grown MoS_2 crystals.[17] We observe the same rubrene film morphology over the SiO_2 substrate as over the 2D WSe_2 crystals, suggesting that rubrene molecular packing was not altered over the atomically smooth surface of the 2D TMD crystals under these deposition conditions.[41] Finally, optical microscopy images surveying larger regions of the sample reveal no discernible breaks or defects in the rubrene:DBP layer covering the 2D WSe_2 crystals (Figures 1d and S3). We note that this ∼1 cm^2-area WSe_2 | rubrene heterostructure has been prepared using industrially relevant CVD and thermal evaporation tools.

We next assessed the steady-state spectral features of the 2D WSe_2 | rubrene heterostructure. We first separately examined the constituents of the heterostructure. Photoluminescence (PL) from our 2D WSe_2 flakes is narrow (115 meV), centered at λ = 775 nm (Figure 1e), and consistent with excitation of the A exciton resonance[45] of the same wavelength in CVD-grown 2D WSe_2. Emission from the rubrene:DBP film is dominated by DBP with three peaks centered at λ = 612, 675, and 725 nm that can be ascribed to the (0 → 0), (0 → 1), and (0 → 2) vibronic transitions reported at the similar wavelengths, respectively.[31,32] Although there are subtle differences between rubrene:DBP emission from solution-cast versus evaporated films,[46] the emission from our films is consistent with that from isolated DBP in solution, which is to be expected given that the DBP concentration in our

https://doi.org/10.1021/acs.nanolett.3c00380
Nano Lett. 2023, 23, 4837−4843

evaporated films is only 1%.[47] PL from the heterostructure (λ_{exc} = 514 nm) reflects a linear combination of the characteristic emission features of each component and is expected based on the steady-state absorption spectrum of the same heterostructure (Figure S4) revealing the unaltered WSe_2 exciton and rubrene absorbance features at 775 nm and between 400 and 600 nm, respectively.[48] These results suggest that the room-temperature optical states of the WSe_2 and rubrene:DBP have not been altered during their assembly into a heterostructure.

To assess the potential of our 2D inorganic−organic heterostructure in solid-state photon upconversion, we examined possible coupling between the band edge states of 2D WSe_2 crystals and the rubrene triplet excited state. To capture the salient photodynamics, time-resolved photoluminescence (TRPL) data were collected on bare 2D WSe_2 crystals and on 2D WSe_2 crystals coated with rubrene:DBP (heterostructures), with λ_{exc} = 730 nm chosen to selectively excite WSe_2 (Figure S4). Here we use a large focal area (>100 μm^2) to obtain the ensemble properties of the sample, rather than the sometimes-variable properties of individual heterostructures defined by single TMD flakes,[36] and to benchmark our results against other film-scale upconversion devices.[24,37]

First, we examined the PL decay dynamics of CVD-grown, monolayer 2D WSe_2 (Figure 2a). We found they are fit well by

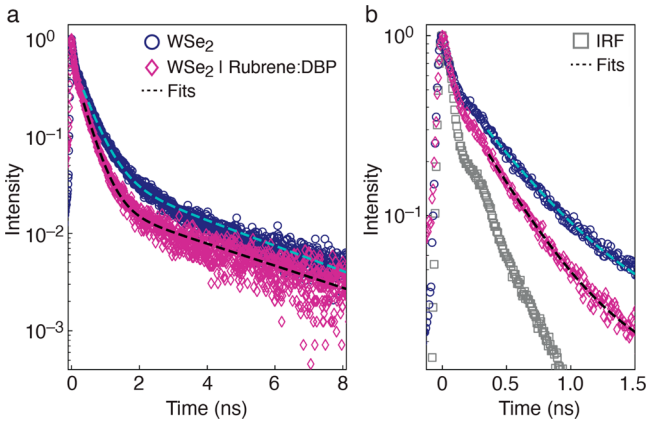

Figure 2. (a) Time-resolved photoluminescence from 2D WSe_2 crystals (blue circles) and 2D WSe_2 | rubrene:DBP heterostructures (pink diamonds) excited at λ = 730 nm. The cyan and black dashed lines are biexponential fits of the WSe_2 and heterostructure data, respectively, over the indicated time range. (b) Time-resolved dynamics from part (a) plotted at earlier times alongside the instrument response function (IRF, gray squares) to highlight the time range (350 ps−1.5 ns) over which they most clearly differ.

a biexponential function in the range 350 ps < t < 8 ns which is chosen to exclude a rapid, initial decay that is obscured by the IRF (Supporting Information Section 4). The lifetimes extracted from the fitted PL data are τ_1 = 440 ± 5 ps and τ_2 = 3.5 ± 0.1 ns and are qualitatively consistent with other reports of PL decay from both CVD-grown and exfoliated TMDs, including WSe_2.[49] The underlying photophysics of these TMD materials is complex and sensitive to the pronounced role of defects that mediate exciton trapping.[50−54] Briefly, PL with a lifetime greater than 1 ns is typically attributed to delayed emission from carriers which were thermally promoted back to the band edge from shallow trap states. Meanwhile, shorter PL lifetimes can be attributed to direct band-edge emission based on studies of monolayer TMD crystals whose traps have been chemically passivated and which exhibit rapid monoexponential PL decay kinetics. The observation that the heterostructure PL dynamics are similar to those of bare 2D WSe_2 beyond 2.5 ns might suggest that some population of atom/nanoscale interfacial voids in the heterostructure lead to areas of effectively bare 2D WSe_2 or that the interfacial transfer of excitations associated with trapped carriers is not effective. The latter possibility contrasts with hypotheses that triplet transfer from some quantum dot sensitizers occurs primarily via surface defects.[55]

Second, we examined the PL dynamics of the WSe_2 | rubrene:DBP heterostructure and observed a significantly shorter lifetime for the first decay component (τ_1 = 350 ± 5 ps) relative to that for bare 2D WSe_2, while the second decay component has marginally longer lifetime (τ_2 = 3.8 ± 0.1 ns) to that measured for bare WSe_2. This decrease in τ_1 is consistent with rapid transfer of free excitons from near the WSe_2 band edge directly to rubrene triplet-excited states before carrier trapping occurs and is in line with previous demonstrations of solid-state molecular triplet sensitization by inorganic semiconductors.[24,51] Comparing the intrinsic (bare WSe_2) and quenched (heterostructure) PL dynamics, we calculate (Supporting Information Section 4) a rate constant of triplet energy transfer (TET) of 5.8 × 10^8 s^{-1} (τ_{TET} = 1.7 ns). Since the dynamics at our shortest time scales are obscured by the instrument response function of the PL measurement (Figure 2b), we used a steady-state PL quenching method to calculate the TET efficiency of the heterostructure as 27% (Figure S5). Given that the thermodynamics for TET are expected to be strongly exothermic, we attribute this modest overall triplet sensitization efficiency to reduced transfer from trap states and/or the presence of the aforementioned interfacial voids. We also note that time-integration of our transient data yields a somewhat lower estimate of the TET efficiency as 18% and suggest that the discrepancy between our calculated efficiencies may point to the presence of sub-ns transfer dynamics in the heterostructure. The presence of such rapid triplet sensitization dynamics would be consistent with the observations of Maiti et al., who used ultrafast transient absorption to study TET from ReS_2 to tetracene, where they note a τ_{TET} of at most 5 ps.[56]

To understand the fate of the WSe_2 to rubrene exciton transfer supported by our TET calculations, we examined steady-state PL spectra collected from the heterostructure. Under 730 nm excitation, we observe fluorescence from the DBP dopant at 610 nm (Figure 3a), which is an unequivocal signature of photon upconversion. We do not observe DBP emission from neat rubrene:DBP films excited at 730 nm (Figure S6). Moreover, on a log−log plot, the slope of the data relating the upconversion emission (λ = 610 nm) to the incident laser intensity shows a transition from 2 to 1 at threshold intensity I_{th} = 110 mW/cm^2 (Figure 3b). This behavior is characteristic of a triplet fusion mechanism, and prior work has outlined the kinetic competitions reflected by this crossover point.[35] Briefly, at lower laser intensities, the relatively sparse volumetric population of triplet excitations in the rubrene layer leaves monomolecular triplet decay processes dominant. As a result, the triplet concentration scales linearly with the excitation intensity, and bimolecular triplet fusion gives the overall quadratic dependence. In contrast, at higher laser intensities, the steady-state population of rubrene triplet excitations is sufficiently high such that second-order triplet

https://doi.org/10.1021/acs.nanolett.3c00380
Nano Lett. 2023, 23, 4837−4843

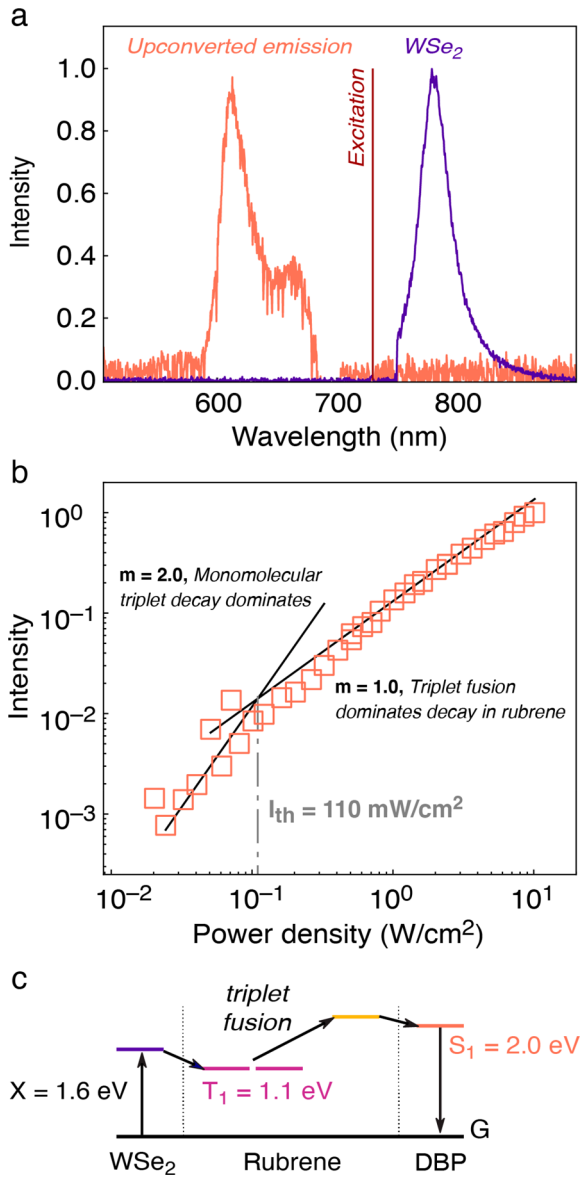

Figure 3. (a) Upconversion emission spectrum (pink) and WSe2 emission spectrum (blue) under continuous-wave λ = 730 nm excitation. (b) Dependence of upconversion emission on laser excitation intensity. The slopes (m) of the data taken within the two decay regimes are identified. (c) Jablonski diagram representing the thermodynamics of the excitation transfer processes in the heterostructure.

fusion becomes dominant and first-order decay processes can be neglected. In this limit, the triplet concentration varies with the square root of the excitation intensity such that the upconverted emission takes on a linear dependence. Furthermore, it is in this regime of high triplet density that the upconversion process reaches its maximum quantum efficiency. Thus, the threshold intensity in steady-state measurements at which the upconverted emission begins to scale linearly with the excitation intensity is a key figure-of-merit.[35,36]

We measured three separate devices, all of which exhibited threshold intensities below 500 mW/cm^2 (Figure S11), thereby demonstrating the reproducibility of the heterostructures prepared by our entirely gas-phase synthesis approach. These included a best performer with a threshold of 110 mW/cm^2 (Figure 3b), which is notable given that this intensity corresponds to 1.1× of the spectrally integrated AM1.5G solar irradiance (Figure S11 and supporting discussion). Despite the relatively low absorption cross-section (<0.1 OD) of the monolayer 2D WSe_2 sensitizer, this threshold value compares to other leading solid-state triplet-fusion upconversion systems based on inorganic semiconductors without photonic enhancement.[32,33] Future heterojunction architectures will maximize light absorption in such material systems to find a path to lower-threshold performance.

To summarize, our data, which reveal a shortened WSe_2 exciton emission lifetime and emission from DBP for 730 nm excitation, are consistent with TET and triplet fusion giving rise to upconversion emission within the heterostructure (Figure 3c). Essentially, excitons at the WSe_2 monolayer band edge are rapidly transferred to the lowest lying spin-triplet state of rubrene (T_1), and triplet fusion yields an excited state in rubrene that has overall singlet spin. Spin-singlet rubrene excitations are then transferred via Förster resonant energy transfer (FRET) to DBP singlets (overcoming the reverse process of singlet fission, 1S → 2T in rubrene), which radiatively recombine to yield the upconverted emission.[31] We note that there is an intriguing contemporary discussion as to the precise nature of the excited state in rubrene following triplet fusion,[31] hence our omission of an explicit label for this state in Figure 3c.

While our calculated value of k_{TET} implies a mechanism of direct exciton transfer to rubrene, we cannot exclude the possibility of single charge carrier transfer. For example, we note that our characteristic time scale of TET is faster than in architectures using nanocrystal sensitizers (>10 ns)[57] and closer to the rapid sensitization observed in perovskite-based devices.[58] By employing a 2D TMD monolayer sensitizer without long-chain alkyl ligands on its surface, we may be overcoming the inherent tunneling barrier experienced by passivated colloidal NCs to facilitate Dexter-type exchange-mediated energy transfer.[57,59,60] It is also possible that the interfacial energy landscape permits a carrier-based, sequential transfer mechanism, as seen in the ultrafast triplet sensitization afforded by bulk perovskites.[32,57,58] Future studies will further examine the photophysics of this 2D TMD/organic vdWH.

Finally, we demonstrate upconversion from large area heterostructures. Adjusting our WSe_2 growth conditions (Supporting Information Section 1) to reduce the nucleation density and bulk oxide deposition affords a nearly continuous crystal film, judging from the uniform optical contrast of the tan-colored regions in Figure 4a. Raman spectra collected at several points within a large area of this sample reveal resonances equivalent to those of isolated 2D WSe_2 monolayers, while AFM height traces reveal a 1 nm thick film (Figure 4a–c). These data reinforce that the tan-colored regions in our bright-field optical images represent the continuous WSe_2 monolayer film. Subsequent analysis of optical images reveals a typical WSe_2 monolayer coverage of 70 ± 8% with coverages as high as 84% attainable over nearly 1 mm^2 areas (Figures S7 and S8; Supporting Information Section). Heterostructures made by evaporating rubrene:DBP over these large-area, continuous films of monolayer WSe_2 produce orange-red upconversion emission that is visible to the naked eye when imaged through a short-pass filter (Figure 4d–e).

https://doi.org/10.1021/acs.nanolett.3c00380
Nano Lett. 2023, 23, 4837−4843

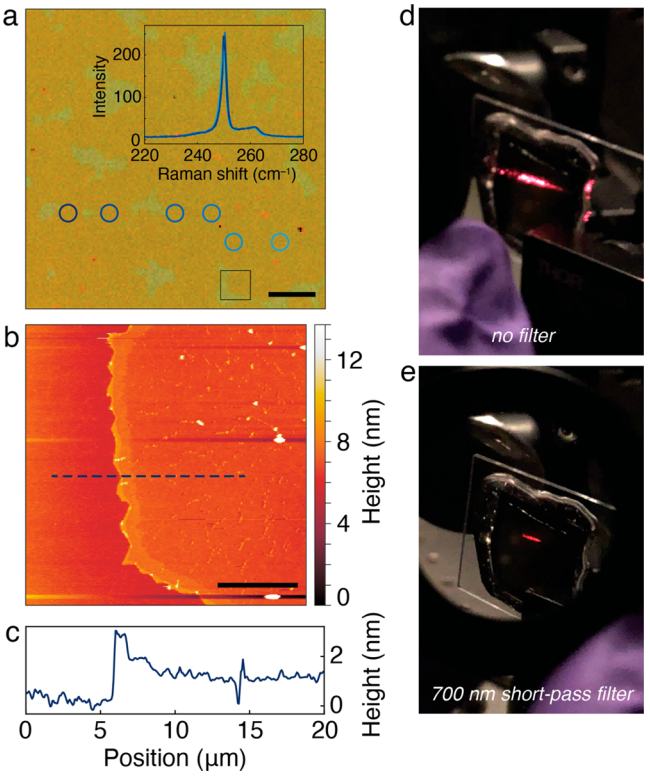

Figure 4. (a) Optical image of a film with ~80% WSe_2 monolayer coverage over an ~0.4 mm^2 area. Inset: Raman spectra collected from the locations outlined with blue circles. Scale bar: 100 μm. (b) AFM map collected within the boxed region in part (a). Scale bar: 10 μm. (c) AFM height trace along the blue line in part (b). (d–e) Photographs of the heterostructure with the laser (λ_{exc} = 730 nm) edge-coupled to the device and taken without (d) and through (e) a 700 nm short-pass filter. Upconversion emission in part (e) is clearly visible to the naked eye from the heterostructure.

In conclusion, we assembled a large area 2D TMD-organic heterostructure and showed that WSe_2 sensitizes triplets in rubrene, leading to a process of triplet fusion upconversion with maximum efficiency threshold at excitation intensities as low as 110 mW/cm^2. We fabricated our heterostructures through entirely gas-phase synthesis and deposition methods, which afford reproducibility in film morphology not only over large areas but also over multiple devices. Demonstrating the scalability and efficiency of our devices, upconversion over several mm^2 areas is visible to the naked eye and occurs at low threshold intensities. We used TRPL to show that our heterostructure, wherein the rubrene acceptor is in close proximity with the 2D crystal monolayer, can facilitate exciton transfer at rates in excess of those observed in colloidal nanocrystal architectures. Our work establishes new opportunities for harnessing multiexciton processes in TMD/organic vdWHs, especially toward device-scale production of heterostructures.

■ ASSOCIATED CONTENT

Supporting Information

The Supporting Information is available free of charge at https://pubs.acs.org/doi/10.1021/acs.nanolett.3c00380.

Supplementary Sections 1–5 containing (i) WSe_2 synthesis and heterostructure fabrication, (ii) optical image analysis for quantifying WSe_2 monolayer coverage, (iii) physical characterization methods, (iv) steady-state and time-resolved spectroscopic methods, and (v) spectroscopic data analysis and Supplementary Figures S1–S11 containing (i) OM images of as-synthesized WSe_2 and heterostructures, (ii) AFM of WSe2 crystals and heterostructures, (iii) absorption spectra, (iv) PL spectra, (v) upconversion intensity power dependence from other devices, and (vi) TRPL data (PDF)

■ AUTHOR INFORMATION

Corresponding Authors

Thomas J. Kempa − *Department of Chemistry, Johns Hopkins University, Baltimore, Maryland 21218, United States; Department of Materials Science & Engineering, Johns Hopkins University, Baltimore, Maryland 21218, United States;* orcid.org/0000-0002-1672-8325; Email: tkempa@jhu.edu

Mark W.B. Wilson − *Department of Chemistry, University of Toronto, Toronto, Ontario M5S 3H6, Canada;* orcid.org/0000-0002-1957-2979; Email: mark.w.b.wilson@utoronto.ca

Authors

Reynolds Dziobek-Garrett − *Department of Chemistry, Johns Hopkins University, Baltimore, Maryland 21218, United States;* orcid.org/0000-0002-8378-1230

Christian J. Imperiale − *Department of Chemistry, University of Toronto, Toronto, Ontario M5S 3H6, Canada;* orcid.org/0000-0001-9504-7394

Complete contact information is available at: https://pubs.acs.org/10.1021/acs.nanolett.3c00380

Author Contributions

[‖]R.D.G. and C.J.I. contributed equally. R.D.G. and C.J.I. performed all experiments with input from M.W.B.W. and T.J.K. All authors contributed to data analyses. The manuscript was written with contributions from all authors. All authors have given approval to the final version of the manuscript.

Funding

T.J.K. acknowledges funding from a National Science Foundation (DMR-1848046) CAREER grant which supported characterization studies in this work. T.J.K. also acknowledges funding for this study by the Young Faculty Award program of the Defense Advanced Research Projects Agency (DARPA) and by the Army Research Office under the grant W911NF-21-1-0351. M.W.B.W. acknowledges the support of the University of Toronto, the Natural Sciences and Engineering Research Council of Canada (NSERC), via RGPIN-2017-06666, and support for research infrastructure from the Canada Foundation for Innovation (JELF-35991) and the Ontario Research Fund (SIA-35991). C.J.I. acknowledges the support of an NSERC PGS-D scholarship.

Notes

The views, opinions, and/or findings expressed are those of the authors and should not be interpreted as representing the official views or policies of the Department of Defense or the U.S. Government.

The authors declare no competing financial interest.

■ ABBREVIATIONS

TMD: transition metal dichalcogenide

CVD: chemical vapor deposition

https://doi.org/10.1021/acs.nanolett.3c00380
Nano Lett. 2023, 23, 4837−4843

PL: photoluminescence
OM: optical microscopy
AFM: atomic force microscopy
TRPL: time-resolved photoluminescence
TUC: triplet fusion upconversion
TET: triplet energy transfer
vdWH: van der Waals heterostructure
DBP: dibenzotetraphenylperiflanthene
Rub: rubrene
2D: two-dimensional
NC: nanocrystal
FRET: Förster resonant energy transfer

REFERENCES

(1) Rivera, P.; Schaibley, J. R.; Jones, A. M.; Ross, J. S.; Wu, S.; Aivazian, G.; Klement, P.; Seyler, K.; Clark, G.; Ghimire, N. J.; Yan, J.; Mandrus, D. G.; Yao, W.; Xu, X. Observation of Long-Lived Interlayer Excitons in Monolayer MoSe 2-WSe 2 Heterostructures. *Nat. Commun.* **2015**, *6*, 6242.

(2) Unuchek, D.; Ciarrocchi, A.; Avsar, A.; Watanabe, K.; Taniguchi, T.; Kis, A. Room-Temperature Electrical Control of Exciton Flux in a van Der Waals Heterostructure. *Nature* **2018**, *560* (7718), 340−344.

(3) Jauregui, L. A.; Joe, A. Y.; Pistunova, K.; Wild, D. S.; High, A. A.; Zhou, Y.; Scuri, G.; de Greve, K.; Sushko, A.; Yu, C. H.; Taniguchi, T.; Watanabe, K.; Needleman, D. J.; Lukin, M. D.; Park, H.; Kim, P. Electrical Control of Interlayer Exciton Dynamics in Atomically Thin Heterostructures. *Science (1979)* **2019**, *366* (6467), 870−875.

(4) Wang, Z.; Rhodes, D. A.; Watanabe, K.; Taniguchi, T.; Hone, J. C.; Shan, J.; Mak, K. F. Evidence of High-Temperature Exciton Condensation in Two-Dimensional Atomic Double Layers. *Nature* **2019**, *574* (7776), 76−80.

(5) Seyler, K. L.; Rivera, P.; Yu, H.; Wilson, N. P.; Ray, E. L.; Mandrus, D. G.; Yan, J.; Yao, W.; Xu, X. Signatures of Moiré-Trapped Valley Excitons in MoSe 2 /WSe 2 Heterobilayers. *Nature* **2019**, *567* (7746), 66−70.

(6) Jin, C.; Regan, E. C.; Yan, A.; Iqbal Bakti Utama, M.; Wang, D.; Zhao, S.; Qin, Y.; Yang, S.; Zheng, Z.; Shi, S.; Watanabe, K.; Taniguchi, T.; Tongay, S.; Zettl, A.; Wang, F. Observation of Moiré Excitons in WSe2/WS2 Heterostructure Superlattices. *Nature* **2019**, *567* (7746), 76−80.

(7) Tran, K.; Moody, G.; Wu, F.; Lu, X.; Choi, J.; Kim, K.; Rai, A.; Sanchez, D. A.; Quan, J.; Singh, A.; Embley, J.; Zepeda, A.; Campbell, M.; Autry, T.; Taniguchi, T.; Watanabe, K.; Lu, N.; Banerjee, S. K.; Silverman, K. L.; Kim, S.; Tutuc, E.; Yang, L.; MacDonald, A. H.; Li, X. Evidence for Moiré Excitons in van Der Waals Heterostructures. *Nature* **2019**, *567* (7746), 71−75.

(8) Bai, Y.; Zhou, L.; Wang, J.; Wu, W.; McGilly, L. J.; Halbertal, D.; Lo, C. F. B.; Liu, F.; Ardelean, J.; Rivera, P.; Finney, N. R.; Yang, X. C.; Basov, D. N.; Yao, W.; Xu, X.; Hone, J.; Pasupathy, A. N.; Zhu, X. Y. Excitons in Strain-Induced One-Dimensional Moiré Potentials at Transition Metal Dichalcogenide Heterojunctions. *Nat. Mater.* **2020**, *19*, 1068.

(9) Yuan, L.; Zheng, B.; Kunstmann, J.; Brumme, T.; Kuc, A. B.; Ma, C.; Deng, S.; Blach, D.; Pan, A.; Huang, L. Twist-Angle-Dependent Interlayer Exciton Diffusion in WS2-WSe2 Heterobilayers. *Nat. Mater.* **2020**, *19* (6), 617−623.

(10) Zhu, X.; Monahan, N. R.; Gong, Z.; Zhu, H.; Williams, K. W.; Nelson, C. A. Charge Transfer Excitons at van Der Waals Interfaces. *J. Am. Chem. Soc.* **2015**, *137* (26), 8313−8320.

(11) Bronstein, H.; Nielsen, C. B.; Schroeder, B. C.; McCulloch, I. The Role of Chemical Design in the Performance of Organic Semiconductors. *Nat. Rev. Chem.* **2020**, *4* (2), 66−77.

(12) Claire, F. J.; Solomos, M. A.; Kim, J.; Wang, G.; Siegler, M. A.; Crommie, M. F.; Kempa, T. J. Structural and Electronic Switching of a Single Crystal 2D Metal-Organic Framework Prepared by Chemical Vapor Deposition. *Nat. Commun.* **2020**, *11* (1), 1−8.

(13) Claire, F. J.; Tenney, S. M.; Li, M. M.; Siegler, M. A.; Wagner, J. S.; Hall, A. S.; Kempa, T. J. Hierarchically Ordered Two-Dimensional Coordination Polymers Assembled from Redox-Active Dimolybdenum Clusters. *J. Am. Chem. Soc.* **2018**, *140* (34), 10673−10676.

(14) Amsterdam, S. H.; Marks, T. J.; Hersam, M. C. Leveraging Molecular Properties to Tailor Mixed-Dimensional Heterostructures beyond Energy Level Alignment. *J. Phys. Chem. Lett.* **2021**, *12* (19), 4543−4557.

(15) Padgaonkar, S.; Olding, J. N.; Lauhon, L. J.; Hersam, M. C.; Weiss, E. A. Emergent Optoelectronic Properties of Mixed-Dimensional Heterojunctions. *Acc. Chem. Res.* **2020**, *53* (4), 763−772.

(16) Jariwala, D.; Marks, T. J.; Hersam, M. C. Mixed-Dimensional van Der Waals Heterostructures. *Nat. Mater.* **2017**, *16*, 170.

(17) Bettis Homan, S.; Sangwan, V. K.; Balla, I.; Bergeron, H.; Weiss, E. A.; Hersam, M. C. Ultrafast Exciton Dissociation and Long-Lived Charge Separation in a Photovoltaic Pentacene-MoS2 van Der Waals Heterojunction. *Nano Lett.* **2017**, *17* (1), 164−169.

(18) Zhong, C.; Sangwan, V. K.; Wang, C.; Bergeron, H.; Hersam, M. C.; Weiss, E. A. Mechanisms of Ultrafast Charge Separation in a PTB7/Monolayer MoS2 van Der Waals Heterojunction. *J. Phys. Chem. Lett.* **2018**, *9* (10), 2484−2491.

(19) Liu, X.; Gu, J.; Ding, K.; Fan, D.; Hu, X.; Tseng, Y. W.; Lee, Y. H.; Menon, V.; Forrest, S. R. Photoresponse of an Organic Semiconductor/Two-Dimensional Transition Metal Dichalcogenide Heterojunction. *Nano Lett.* **2017**, *17* (5), 3176−3181.

(20) Li, S.; Zhong, C.; Henning, A.; Sangwan, V. K.; Zhou, Q.; Liu, X.; Rahn, M. S.; Wells, S. A.; Park, H. Y.; Luxa, J.; Sofer, Z.; Facchetti, A.; Darancet, P.; Marks, T. J.; Lauhon, L. J.; Weiss, E. A.; Hersam, M. C. Molecular-Scale Characterization of Photoinduced Charge Separation in Mixed-Dimensional InSe-Organic van Der Waals Heterostructures. *ACS Nano* **2020**, *14* (3), 3509−3518.

(21) Cheng, C. H.; Li, Z.; Hambarde, A.; Deotare, P. B. Efficient Energy Transfer across Organic-2D Inorganic Heterointerfaces. *ACS Appl. Mater. Interfaces* **2018**, *10* (45), 39336−39342.

(22) Qian, Q.; Ren, H.; Zhou, J.; Wan, Z.; Zhou, J.; Yan, X.; Cai, J.; Wang, P.; Li, B.; Sofer, Z.; Li, B.; Duan, X.; Pan, X.; Huang, Y.; Duan, X. Chiral Molecular Intercalation Superlattices. *Nature* **2022**, *606* (7916), 902−908.

(23) Duan, J.; Liu, Y.; Zhang, Y.; Chen, Z.; Xu, X.; Ye, L.; Wang, Z.; Yang, Y.; Zhang, D.; Zhu, H. Efficient Solid-State Infrared-to-Visible Photon Upconversion on Atomically Thin Monolayer Semiconductors. *Sci. Adv.* **2022**, *8* (43), No. eabq4935.

(24) Singh-Rachford, T. N.; Castellano, F. N. Photon Upconversion Based on Sensitized Triplet-Triplet Annihilation. *Coord. Chem. Rev.* **2010**, *254* (21−22), 2560−2573.

(25) Zhou, J.; Liu, Q.; Feng, W.; Sun, Y.; Li, F. Upconversion Luminescent Materials: Advances and Applications. *Chem. Rev.* **2015**, *115* (1), 395−465.

(26) Zhou, Y.; Castellano, F. N.; Schmidt, T. W.; Hanson, K. On the Quantum Yield of Photon Upconversion via Triplet-Triplet Annihilation. *ACS Energy Lett.* **2020**, *5* (7), 2322−2326.

(27) Najafov, H.; Lee, B.; Zhou, Q.; Feldman, L. C.; Podzorov, V. Observation of Long-Range Exciton Diffusion in Highly Ordered Organic Semiconductors. *Nat. Mater.* **2010**, *9* (11), 938−943.

(28) Li, X.; Tang, M. L. Triplet Transport in Thin Films: Fundamentals and Applications. *Chem. Commun.* **2017**, *53* (32), 4429−4440.

(29) Wolf, E. A.; Biaggio, I. Geminate Exciton Fusion Fluorescence as a Probe of Triplet Exciton Transport after Singlet Fission. *Phys. Rev. B* **2021**, *103* (20), L201201.

(30) Köhler, A.; Bässler, H. Triplet States in Organic Semiconductors. *Materials Science and Engineering: R: Reports* **2009**, *66* (4−6), 71−109.

(31) Bossanyi, D. G.; Sasaki, Y.; Wang, S.; Chekulaev, D.; Kimizuka, N.; Yanai, N.; Clark, J. In Optimized Rubrene-Based Nanoparticle Blends for Photon Upconversion, Singlet Energy Collection Outcompetes Triplet-Pair Separation, Not Singlet Fission. *J. Mater. Chem. C Mater.* **2022**, *10* (12), 4684−4696.

(32) Wu, M.; Congreve, D. N.; Wilson, M. W. B.; Jean, J.; Geva, N.; Welborn, M.; Van Voorhis, T.; Bulovic, V.; Bawendi, M. G.; Baldo, M.

https://doi.org/10.1021/acs.nanolett.3c00380
Nano Lett. 2023, 23, 4837−4843

A. Solid-State Infrared-to-Visible Upconversion Sensitized by Colloidal Nanocrystals. *Nat. Photonics* **2016**, *10* (1), 31−34.
(33) Wieghold, S.; Bieber, A. S.; VanOrman, Z. A.; Daley, L.; Leger, M.; Correa-Baena, J. P.; Nienhaus, L. Triplet Sensitization by Lead Halide Perovskite Thin Films for Efficient Solid-State Photon Upconversion at Subsolar Fluxes. *Matter* **2019**, *1* (3), 705−719.
(34) Ha, D. G.; Wan, R.; Kim, C. A.; Lin, T. A.; Yang, L.; van Voorhis, T.; Baldo, M. A.; Dincă, M. Exchange Controlled Triplet Fusion in Metal-Organic Frameworks. *Nat. Mater.* **2022**, *21* (11), 1275−1281.
(35) Haefele, A.; Blumhoff, J.; Khnayzer, R. S.; Castellano, F. N. Getting to the (Square) Root of the Problem: How to Make Noncoherent Pumped Upconversion Linear. *J. Phys. Chem. Lett.* **2012**, *3* (3), 299−303.
(36) Schmidt, T. W.; Castellano, F. N. Photochemical Upconversion: The Primacy of Kinetics. *J. Phys. Chem. Lett.* **2014**, *5* (22), 4062−4072.
(37) Hoseinkhani, S.; Tubino, R.; Meinardi, F.; Monguzzi, A. Achieving the Photon Up-Conversion Thermodynamic Yield Upper Limit by Sensitized Triplet-Triplet Annihilation. *Phys. Chem. Chem. Phys.* **2015**, *17* (6), 4020−4024.
(38) Duan, P.; Yanai, N.; Nagatomi, H.; Kimizuka, N. Photon Upconversion in Supramolecular Gel Matrixes: Spontaneous Accumulation of Light-Harvesting Donor-Acceptor Arrays in Nanofibers and Acquired Air Stability. *J. Am. Chem. Soc.* **2015**, *137* (5), 1887−1894.
(39) Monguzzi, A.; Tubino, R.; Meinardi, F. Multicomponent Polymeric Film for Red to Green Low Power Sensitized Up-Conversion. *J. Phys. Chem. A* **2009**, *113* (7), 1171−1174.
(40) Bernardi, M.; Palummo, M.; Grossman, J. C. Extraordinary Sunlight Absorption and One Nanometer Thick Photovoltaics Using Two-Dimensional Monolayer Materials. *Nano Lett.* **2013**, *13* (8), 3664−3670.
(41) Wang, G.; Chernikov, A.; Glazov, M. M.; Heinz, T. F.; Marie, X.; Amand, T.; Urbaszek, B. Colloquium : Excitons in Atomically Thin Transition Metal Dichalcogenides. *Rev. Mod. Phys.* **2018**, *90* (2), 21001.
(42) Kafle, T. R.; Kattel, B.; Lane, S. D.; Wang, T.; Zhao, H.; Chan, W. L. Charge Transfer Exciton and Spin Flipping at Organic-Transition-Metal Dichalcogenide Interfaces. *ACS Nano* **2017**, *11* (10), 10184−10192.
(43) Sahin, H.; Tongay, S.; Horzum, S.; Fan, W.; Zhou, J.; Li, J.; Wu, J.; Peeters, F. M. Anomalous Raman Spectra and Thickness-Dependent Electronic Properties of WSe2. *Phys. Rev. B* **2013**, *87* (16), 165409.
(44) Kondakov, D. Y.; Pawlik, T. D.; Hatwar, T. K.; Spindler, J. P. Triplet Annihilation Exceeding Spin Statistical Limit in Highly Efficient Fluorescent Organic Light-Emitting Diodes. *J. Appl. Phys.* **2009**, *106* (12), 124510.
(45) Huang, J. K.; Pu, J.; Hsu, C. L.; Chiu, M. H.; Juang, Z. Y.; Chang, Y. H.; Chang, W. H.; Iwasa, Y.; Takenobu, T.; Li, L. J. Large-Area Synthesis of Highly Crystalline WSe2Monolayers and Device Applications. *ACS Nano* **2014**, *8* (1), 923−930.
(46) Wieghold, S.; Bieber, A. S.; Vanorman, Z. A.; Rodriguez, A.; Nienhaus, L. Is Disorder Beneficial in Perovskite-Sensitized Solid-State Upconversion? The Role of DBP Doping in Rubrene. *J. Phys. Chem. C* **2020**, *124* (33), 18132−18140.
(47) Debad, J. D.; Morris, J. C.; Lynch, V.; Magnus, P.; Bard, A. J. Dibenzotetraphenylperiflanthene: Synthesis, Photophysical Properties, and Electrogenerated Chemiluminescence. *J. Am. Chem. Soc.* **1996**, *118* (10), 2374−2379.
(48) Najafov, H.; Biaggio, I.; Podzorov, V.; Calhoun, M. F.; Gershenson, M. E. Primary Photoexcitations and the Origin of the Photocurrent in Rubrene Single Crystals. *Phys. Rev. Lett.* **2006**, *96* (5), 056604.
(49) Kim, H.; Ahn, G. H.; Cho, J.; Amani, M.; Mastandrea, J. P.; Groschner, C. K.; Lien, D. H.; Zhao, Y.; Ager, J. W.; Scott, M. C.; Chrzan, D. C.; Javey, A. Synthetic WSe 2 Monolayers with High Photoluminescence Quantum Yield. *Sci. Adv.* **2019**, *5* (1), eaau4728.
(50) Tanoh, A. O. A.; Alexander-Webber, J.; Xiao, J.; Delport, G.; Williams, C. A.; Bretscher, H.; Gauriot, N.; Allardice, J.; Pandya, R.; Fan, Y.; Li, Z.; Vignolini, S.; Stranks, S. D.; Hofmann, S.; Rao, A. Enhancing Photoluminescence and Mobilities in WS2Monolayers with Oleic Acid Ligands. *Nano Lett.* **2019**, *19* (9), 6299−6307.
(51) Tanoh, A. O. A.; Alexander-Webber, J.; Fan, Y.; Gauriot, N.; Xiao, J.; Pandya, R.; Li, Z.; Hofmann, S.; Rao, A. Giant Photoluminescence Enhancement in MoSe 2 Monolayers Treated with Oleic Acid Ligands. *Nanoscale Adv.* **2021**, *3* (14), 4216−4225.
(52) Goodman, A. J.; Lien, D. H.; Ahn, G. H.; Spiegel, L. L.; Amani, M.; Willard, A. P.; Javey, A.; Tisdale, W. A. Substrate-Dependent Exciton Diffusion and Annihilation in Chemically Treated MoS2 and WS2. *J. Phys. Chem. C* **2020**, *124* (22), 12175−12184.
(53) Amani, M.; Lien, D.; Kiriya, D.; Xiao, J.; Azcatl, A.; Noh, J.; Madhvapathy, S. R.; Addou, R.; Dubey, M.; Cho, K.; Wallace, R. M.; Lee, S.; He, J.; Zhang, X.; Yablonovitch, E.; Javey, A.; KC, S.; Ager, J. W. Near-Unity Photoluminescence Quantum Yield in MoS 2. *Science (1979)* **2015**, *350* (6264), 1065.
(54) Li, Z.; Bretscher, H.; Zhang, Y.; Delport, G.; Xiao, J.; Lee, A.; Stranks, S. D.; Rao, A. Mechanistic Insight into the Chemical Treatments of Monolayer Transition Metal Disulfides for Photoluminescence Enhancement. *Nat. Commun.* **2021**, *12* (1), 6044.
(55) Bender, J. A.; Raulerson, E. K.; Li, X.; Goldzak, T.; Xia, P.; van Voorhis, T.; Tang, M. L.; Roberts, S. T. Surface States Mediate Triplet Energy Transfer in Nanocrystal-Acene Composite Systems. *J. Am. Chem. Soc.* **2018**, *140* (24), 7543−7553.
(56) Maiti, S.; Poonia, D.; Schiettecatte, P.; Hens, Z.; Geiregat, P.; Kinge, S.; Siebbeles, L. D. A. Generating Triplets in Organic Semiconductor Tetracene upon Photoexcitation of Transition Metal Dichalcogenide ReS2. *J. Phys. Chem. Lett.* **2021**, *12* (22), 5256−5260.
(57) Nienhaus, L.; Wu, M.; Geva, N.; Shepherd, J. J.; Wilson, M. W. B.; Bulović, V.; van Voorhis, T.; Baldo, M. A.; Bawendi, M. G. Speed Limit for Triplet-Exciton Transfer in Solid-State PbS Nanocrystal-Sensitized Photon Upconversion. *ACS Nano* **2017**, *11* (8), 7848−7857.
(58) Nienhaus, L.; Correa-Baena, J. P.; Wieghold, S.; Einzinger, M.; Lin, T. A.; Shulenberger, K. E.; Klein, N. D.; Wu, M.; Bulović, V.; Buonassisi, T.; Baldo, M. A.; Bawendi, M. G. Triplet-Sensitization by Lead Halide Perovskite Thin Films for near-Infrared-to-Visible Upconversion. *ACS Energy Lett.* **2019**, *4* (4), 888−895.
(59) Dexter, D. L. A Theory of Sensitized Luminescence in Solids. *J. Chem. Phys.* **1953**, *21* (5), 836.
(60) Lai, R.; Liu, Y.; Luo, X.; Chen, L.; Han, Y.; Lv, M.; Liang, G.; Chen, J.; Zhang, C.; Di, D.; Scholes, G. D.; Castellano, F. N.; Wu, K. Shallow Distance-Dependent Triplet Energy Migration Mediated by Endothermic Charge-Transfer. *Nature Communications* **2021**, *12*, 1532.

https://doi.org/10.1021/acs.nanolett.3c00380
Nano Lett. 2023, 23, 4837−4843